Supplementary Materials for

Cenozoic evolution of deep ocean temperature from clumped isotope thermometry

A. N. Meckler *et al.*

Corresponding author: A. N. Meckler, nele.meckler@uib.no

Science **377**, 86 (2022)
DOI: 10.1126/science.abk0604

The PDF file includes:

Materials and Methods
Figs. S1 to S7
Tables S1 and S2
References

Other Supplementary Material for this manuscript includes the following:

Data S1 to S3

Materials and Methods

Material

1. Newfoundland Margin

Large individual samples, for the most part core catchers, were taken from four different International Ocean Discovery Program (IODP) sites recovered by Expedition 342 on the Newfoundland margin in the North Atlantic (1406, 1407, 1409, and 1410; Table S1, Fig. S1), together covering the entire Cenozoic era (*44*). Age models for all Sites are based on detailed integrated bio-magneto-stratigraphies (*44*), updated to the CENOGRID timescale (*2*). Other supporting datasets that we show in Figures 1 and 2 (atmospheric CO_2 and previous estimates of deep ocean temperature and $\delta^{18}O_{sw}$) are plotted on their published age models; minor resulting differences in age models are not relevant on the timescales investigated here.

For each sample, benthic foraminifera were picked from size fractions >150 µm. A large variety of foraminifer species were used for analysis in order to achieve the necessary level of replication (Data S2), whereby aliquots for measurements were separated on the species or at least genus level where possible. Aliquots were cleaned by carefully opening foraminifera tests, followed by several iterations of ultrasonication using both deionized water and methanol, with subsequent rinses with deionized water and oven-drying at 50°C.

Scanning electron microscope images were obtained from a random selection of cleaned sample aliquots distributed over the whole study interval (Fig. S2).

2. Walvis Ridge

For the Early Eocene, one additional clumped isotope temperature was obtained from Site 1263 (paleo-water depth ~1500 m) on the Walvis Ridge in the South Atlantic as an average of analyses from multiple individual samples spanning ~400 kyr (from 51.3 to 50.9 Ma). Foraminifer species *Nuttalides truempyi* and *Oridorsalis umbonatus* from the > 150 µm size fraction were cleaned and analyzed at Utrecht University.

Methods

1. Clumped isotope thermometry

Clumped isotope thermometry takes advantage of the temperature dependence of isotopic ordering within molecules, with double substitution by heavy isotopes (e.g., ^{18}O and ^{13}C in carbonates) increasing with decreasing formation temperature (*13*). The excess abundance of such double substitution in carbonates compared to random ordering (Δ_{47}) is independent of the composition of the source water. The signal furthermore does not exhibit biological effects in foraminifera (*46-50*), appears to not be measurably affected by seawater pH within the range typical for the ocean (*28, 30*), and is largely robust to diagenetic overprinting in benthic foraminifera from typical ocean settings (*19*), if burial depth was sufficiently shallow (*51*). Using carbonate-based standardization

(*52*), calibrations can be reproduced in different laboratories, and foraminifera-based calibrations are indistinguishable from inorganically precipitated calcite (*46, 47, 50*). The comparatively large analytical uncertainty due to a small signal-to-noise ratio can be mitigated by extensive replication, where sample availability permits.

Clumped isotope measurements were performed between 2015 and 2020 on four different mass spectrometers in Bergen, Zürich, and Utrecht, all consisting of Thermo Fisher Scientific MAT253 or MAT253Plus instruments coupled to Thermo Fisher Scientific Kiel IV carbonate preparation devices. Most of the analyses (N = 936) were performed on two different mass spectrometers in Bergen, with the exception of some North Atlantic sample aliquots measured in Zürich (N = 43), and early Eocene samples from Walvis Ridge analyzed in Utrecht (N = 61). The analytical approach was similar to that described by (*53*) and updated for the Bergen analyses as described by (*49*) and (*46*). The methodological details for the Utrecht lab are described in (*18*). In the Kiel device, sample aliquots are individually reacted with phosphoric acid at 70°C, and the sample gas is cryogenically separated from water and other trace gases. All Kiel devices were equipped with additional custom-built traps for organic contaminants (Porapak Q columns, held at -20°C; -45°C in the Utrecht lab) and sulfide components (Ag wool). All measurements were conducted in microvolume mode, and in the case of the Bergen and Utrecht instruments, the long-integration-dual-inlet method (LIDI; *54*) was used. Masses 44-49 were monitored, and masses 44-47 were used for calculating $\delta^{13}C$, $\delta^{18}O$, and Δ_{47}. The raw data were corrected for pressure baseline effects based on daily peak scans (*53*) and further corrections for Δ_{47} scale compression and transfer to the I-CDES scale (*55*) were made using carbonate standards ETH 1-3. The accepted values of these standards were derived by multiple laboratories (*55*) and reported for an acid digestion temperature of 90 °C. Our $\Delta_{47\ (I\text{-}CDES)}$ results therefore also reflect an acid digestion temperature 90 °C (but note that by using carbonate standards, no acid fractionation factor needs to be applied). Standard aliquots were measured in roughly equal numbers as sample aliquots. In most cases, a moving window approach was used to base corrections on standard data from several adjacent days, with the number of standard measurements used for corrections depending on instrument stability. For the measurements performed in Bergen, data corrections were done with the Easotope software (*56*). All replicate-level data are archived in the Earthchem database (*41, 42*), including information regarding standard correction procedures. Sample-averaged data are reported as Data S1 and are archived in the Pangaea database (*43*).

Final corrected Δ_{47} values on the I-CDES scale were averaged per sample, before temperatures were calculated using the combined foraminifera-based calibration of (*46*), updated to the I-CDES scale by (*57*), that is based on three different calibration datasets measured in two different laboratories:

$$\Delta_{47}(I - CDES) = (0.0397\ \pm 0.0011) * \frac{10^6}{T^2} + (0.1518\ \pm 0.0128)$$

Thereby, temperature is given in °K. Choosing a different calibration has only a small effect on the results (Fig. S3), as long as calibrations are based on the same carbonate standardization approach. We tested i) the travertine-based calibration of (*58*), as recalculated by (*52*), using Δ_{47} from our samples standardized to the original values of the ETH standards published by (*52*), and ii) the combined inorganic-biogenic carbonate calibration of (*59*) covering a temperature range of more than 1000 °C. The differences between temperatures calculated with these equations and our preferred approach are -1.0 to 0.9 °C for (i) and -1.9 °C for (ii). For this study, we chose to use the foraminifera-based calibration (*46*), as it contains most foraminifera data, treats these in a consistent way (e.g., calculation of calcification temperatures), and has a larger data density in the interval of ocean temperatures compared to the travertine calibration. It furthermore avoids the influence of analytical uncertainty of sparse measurements on high-temperature samples and possible effects of the Δ_{47} dependence on temperature deviating from a linear relationship with $1/T^2$ over large temperature ranges (*60*).

All temperatures are plotted with 68% and 95% confidence intervals on the average temperatures, which combine the analytical uncertainty and the calibration uncertainty of (*46;* their Fig. A2), updated by (*57*) using a Monte Carlo approach that samples a random slope-intercept pair for the calibration and a random Δ_{47} value from their respective probability distributions (5000 iterations). In addition, the number of replicates is indicated by different gray shading in order to optically give more weight to the better replicated analyses. LOESS smoothing was applied to the full North Atlantic temperature data set, taking into account the confidence levels of each data point. Assuming normal distribution of errors, we applied a Monte Carlo method to generate 10,000 realizations of the temperature time series. A LOESS curve (span = 0.2, degree = 1) was then fitted to each of the 10,000 realizations. These LOESS fits served as a basis for calculating 95% confidence intervals (2.5 and 97.5 percentiles; gray shading in Figures 1 and 2).

2. $\delta^{13}C$, $\delta^{18}O$, $\delta^{18}O_{sw}$

$\delta^{13}C$ and $\delta^{18}O$ values were calibrated to the Vienna Pee Dee Belemnite (VPDB) scale with the ETH 1-4 carbonate standards that were also used for Δ_{47} corrections in a similar moving window approach with standard results from several days. The clumped isotope standards have previously been calibrated to the VPDB scale using the international carbonate standards NBS-18, NBS-19, and LSVEC (*52*). In the case of $\delta^{18}O$, the standard correction also accounted for minor variations in $\delta^{18}O$ scale compression.

$\delta^{18}O_{sw}$ was calculated from the Δ_{47} temperatures and the $\delta^{18}O_b$ values determined from *Cibicidoides spec.*, using a temperature- $\delta^{18}O_b$ relationship derived for that genus (*7;* their equation 9). For early Eocene data from Walvis Ridge and Maud Rise, where *Cibicidoides* were not measured, $\delta^{18}O_b$ from *Nuttalides* and *Oridorsalis* were first corrected for inter-species offsets from *Cibicidoides* using the relationships suggested by (*9*).

3. Deep Ocean pH

Boron isotope data from benthic foraminifera were generated from the North Atlantic (U1409) and Central Atlantic (ODP 1258 and 1260, 45-52 Ma) and combined with published data from the Central Atlantic (ODP 999 and 926; *40*) – see Table S2 for details. These sites span paleo-depths from 2.5-3.6 km, which are today bathed by northern-sourced waters with similar properties (*61*), and we find consistent values between sites in our record. Analyses were made on mono-specific samples of the genus *Cibicidoides*: *C. wuellerstorfi* and *C. mundulus* in the Neogene and *C. eocaenus*, *C. havanensis*, and *C. velascoensis* in the Paleogene.

Analytical methods followed established protocols (e.g., *62-64*). In brief, foraminifera were crushed, oxidatively cleaned with hydrogen peroxide, and dissolved following (*62*). A small split (<5 %) of the sample was analyzed for minor and trace element composition by ICPMS to assess boron content and sample cleanliness. Boron was then removed from the sample matrix, using ion exchange column chromatography with Amberlite 743, and analyzed by MC-ICPMS. Data were obtained from site U1409 in the St Andrews isotope Geochemistry (STAiG) laboratories at the University of St Andrews and from sites 1258 and 1260 in the Bristol Isotope Group (BIG) at the University of Bristol. Analyses in these laboratories follow very similar protocols, though with some minor differences (boron washout assisted using NH_3 at BIG, HF at STAiG; and signal detection using 10^{11} Ω amplifiers at BIG, 10^{13} Ω amplifiers at STAiG). Cross calibration between these laboratories has been ensured by participation in interlaboratory comparison exercises (*64-66*) and use of identical primary and consistency standards, yielding consistent values (e.g. the pooled 2SD of boric acid consistency standards measured across both laboratories during these analytical sessions is 0.17 ‰, n=8). Uncertainties are reported at 2SD based on long-term reproducibility of samples of this size in each lab.

Calculation of deep ocean pH as shown in Figure 2C follows the procedures in (*67*) and (*24*). We assume that these epifaunal *Cibicidoides* species record bottom water $\delta^{11}B$ of borate, as seen in modern calibrations (*62*). To calculate the boric acid dissociation constant (K_B) we interpolate the smoothed clumped isotope temperature record presented here (Fig. 1A), use salinity of 35, paleo water depths as shown in Table S2 (noting that depth and salinity have little influence on calculated pH), and we account for the (minor) influence of changing seawater [Ca^{2+}] and [Mg^{2+}] (e.g., *68*) using MyAMI (*69*) as in (*24*). We use the compilation of $\delta^{11}B_{SW}$ estimates from (*24*). The influence of ±0.5 ‰ in $\delta^{11}B_{SW}$ on pH is shown with the shaded area in Figure 2C and the influence of analytical uncertainties in $\delta^{11}B$ and ± 2 °C in temperature are shown by the 2SD error bars, based on the standard deviation of a 10,000 member Monte Carlo ensemble.

The deep ocean pH data are reported as Data S3 and archived in the Earthchem and Pangaea databases.

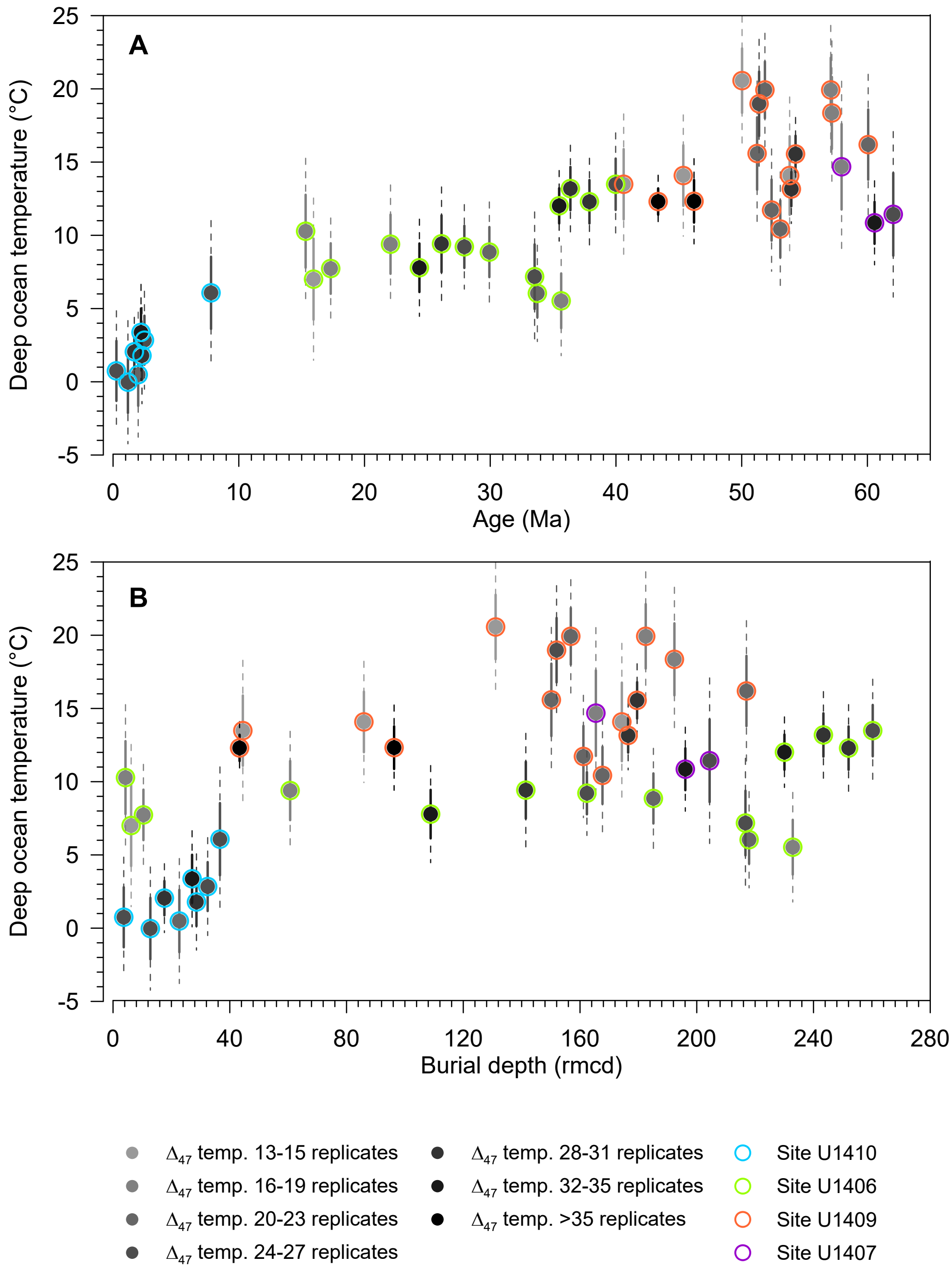

Fig. S1: North Atlantic IODP Expedition 342 Sites used for the different parts of the record (A) and clumped isotope temperatures versus burial depth (B). Note the close reproducibility of temperatures at 40 Ma, with overlapping data from two sites with very different burial depths in each (1406B core 28 at 260 m vs. 1409C core 5 at 44 m). See also the respective SEM images of foraminifer tests from each of these two samples in Figure S2. Burial depth is given in revised meter composite depth (rmcd; *44*). We do not observe a consistent relationship between clumped isotope temperatures and burial depth (panel B).

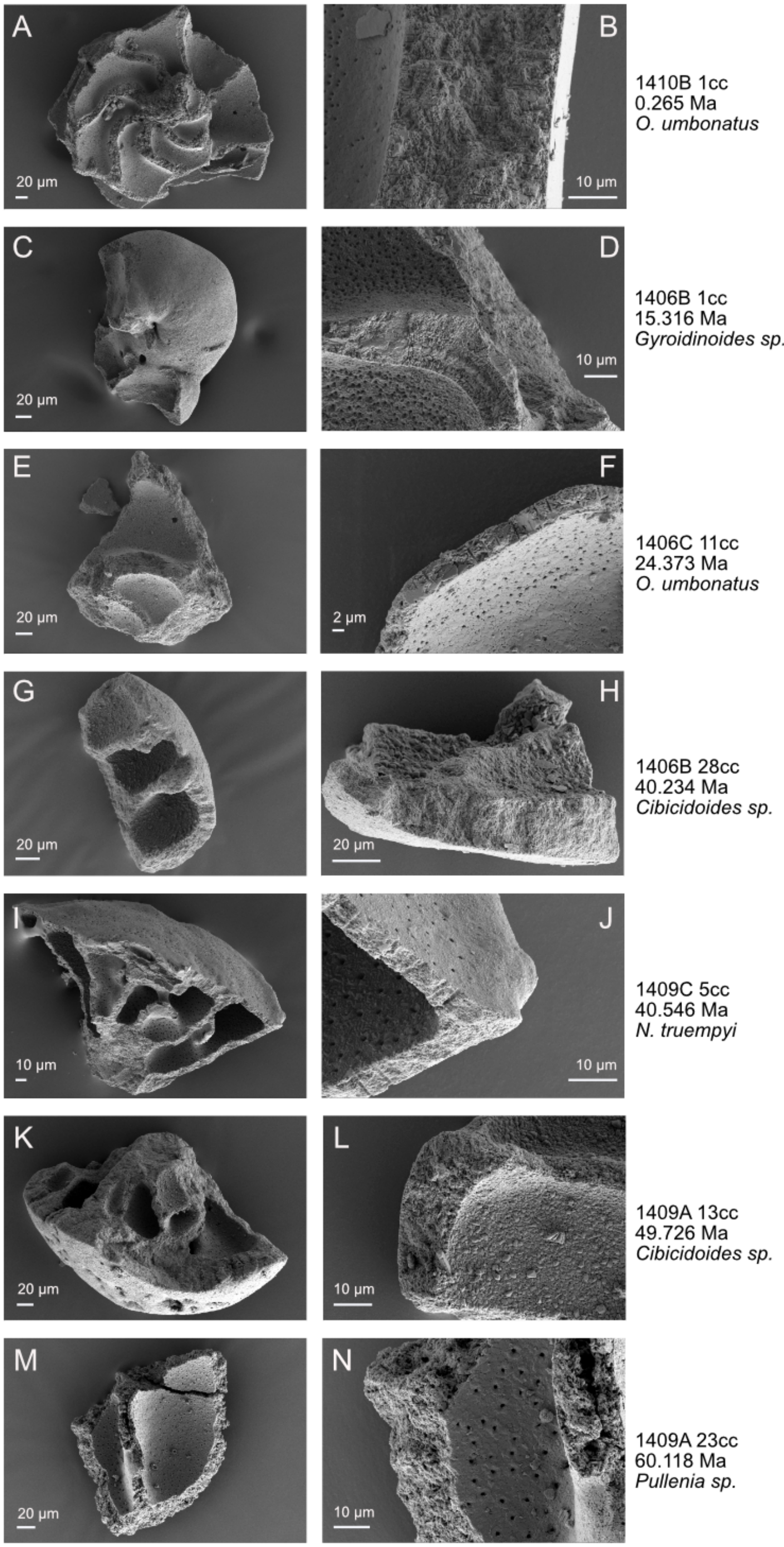

Fig. S2. SEM images of benthic foraminifera analyzed for clumped isotopes spanning the Cenozoic record.

Preservation state is generally good to excellent (clearly visible microstructures such as pores and layered structure of wall cross-sections) but shows the expected deterioration (addition of blocky calcite overgrowth) with depth (increasing core number X in "Xcc"). Note for example the different extent of overgrowth on two samples for ~40 Ma stemming from different sites and burial depths (G, H vs. I, J). The sample from 1406B 28cc shows blocky calcite overgrowth on the inside of the shell fragment (H), which is not observed on the fragment from 1409C 5cc (J). These samples yielded nonetheless indistinguishable temperatures.

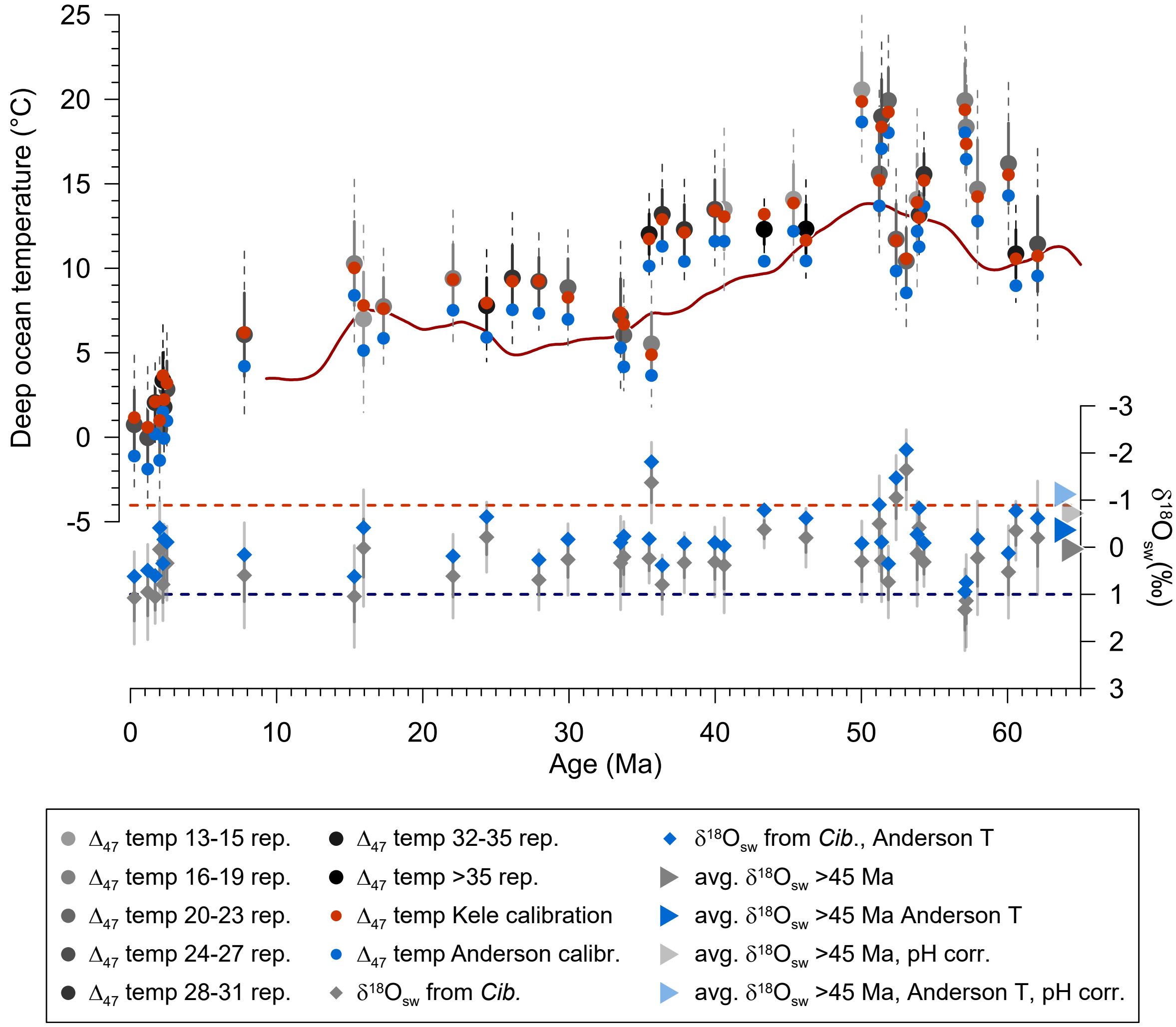

Fig. S3. Influence of different clumped isotope calibration on reconstructed temperatures and $\delta^{18}O_{sw}$. The calibration used in this study is based on a compilation of planktic and benthic foraminifera from surface sediments (*46*), updated to the I-CDES scale by (*57*). The gray symbols in the top and bottom panels represent the North Atlantic data calculated with this calibration and are the same as shown in Figs. 1A and 2A and in Fig. 2D, respectively. The results match well to the temperatures obtained when using a calibration based on travertines and tufas covering a larger temperature range ("Kele calibration" (*58*), recalculated by (*52*)) with differences of -1.0 to 0.9 °C. The differences to this calibration include the effects of slightly different standardization (CDES versus I-CDES scale). A recent calibration covering a temperature range of 1000°C and including previous calibration data including most, but not all, of the above (*59*), on the other hand yields temperatures slightly colder (by 1.9 °C), but the general observations remain unchanged. With this ("Anderson") calibration, $\delta^{18}O_{sw}$ is 0.4 ‰ heavier (blue symbols in bottom panel). Average $\delta^{18}O_{sw}$ for >45 Ma (arrows to the right) with and without a pH correction become -1.13 ‰ and -0.37 ‰, respectively.

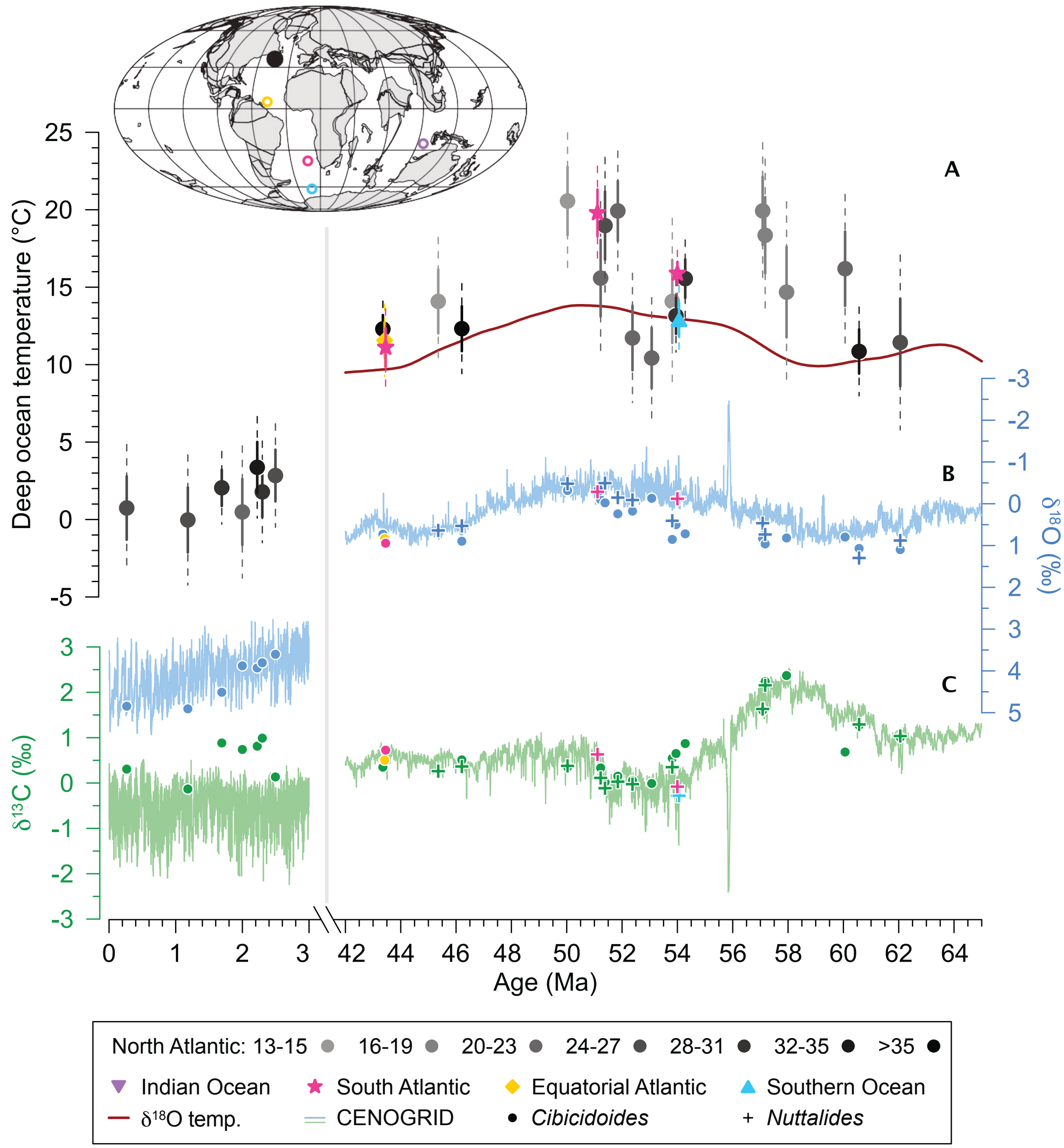

Fig. S4. Close-up of the early and late Cenozoic intervals of Fig. 1. As explained in the caption for Fig. 1, some of the apparent offsets in $\delta^{18}O_b$ and $\delta^{13}C$ between our data and CENOGRID (*2*) are due to adjustments for inter-site/basin offsets in the CENOGRID data set. For example, the South Atlantic data used for most of the Paleocene and early Eocene sections of the CENOGRID record have been adjusted by -0.2 ‰ (*2*), but such a correction was not applied to our data for lack of constraints.

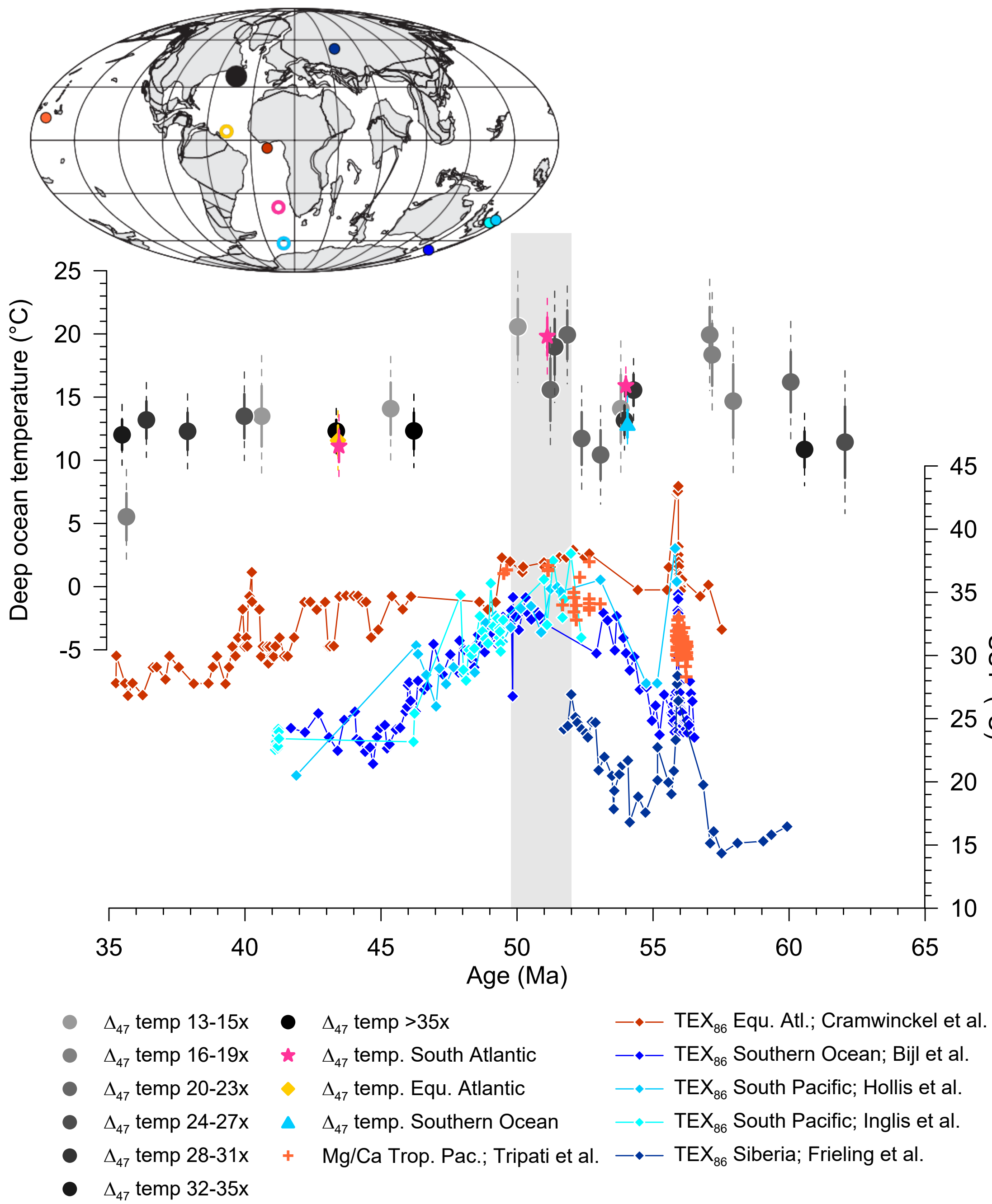

Fig. S5. Comparison of deep ocean temperatures for the early Cenozoic with the most detailed sea surface temperature (SST) records currently available. Most SST records that span a significant time period in the Early Cenozoic with sufficient resolution are based on organic biomarkers (TEX_{86} proxy). The SST data shown here (*70-78*) were obtained from a recent compilation of early Cenozoic temperature data (*8*) and age models were updated to the CENOGRID timescale for direct comparison to our data. The gray bar highlights the early Eocene interval of elevated Atlantic deep ocean temperatures. The locations of the SST sites are indicated on the inset map by closed small circles.

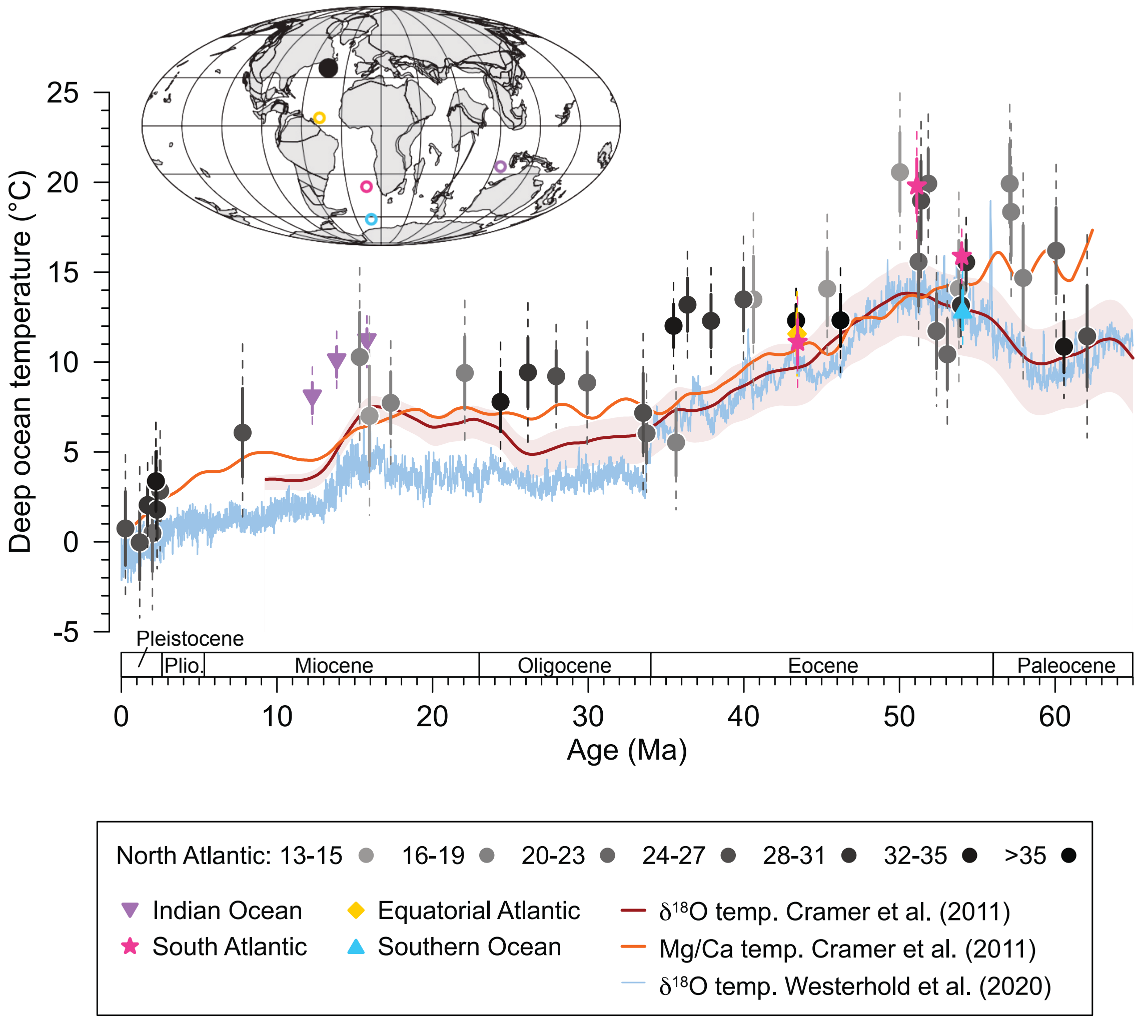

Fig. S6. Comparison of clumped isotope temperatures to estimates of deep ocean temperature based on $\delta^{18}O$ and Mg/Ca. Red line with uncertainty band: temperature estimate based on $\delta^{18}O_b$ and reconstructed sea level (*6*); Orange line: Mg/Ca-based temperature record (*6),* in the version using Equation 7b of (*6*) for temperature calculation. This reconstruction is based on a global compilation of selected Mg/Ca records, but in the Paleocene to middle Eocene is based on sparse data predominantly from the Pacific Ocean. Light blue line: CENOGRID $\delta^{18}O_b$ -based deep ocean temperature (*2*) calculated with the approach suggested by Hansen (*79*), which accounts for the varying contribution of ice sheet size by defining three different equations for different time intervals (0-3.6 Ma, 3.6-34 Ma, and prior to 34 Ma). Gray and colored symbols: Clumped isotope temperatures with uncertainties as in Figs. 1 and 2. Previous estimates are plotted on their published age models.

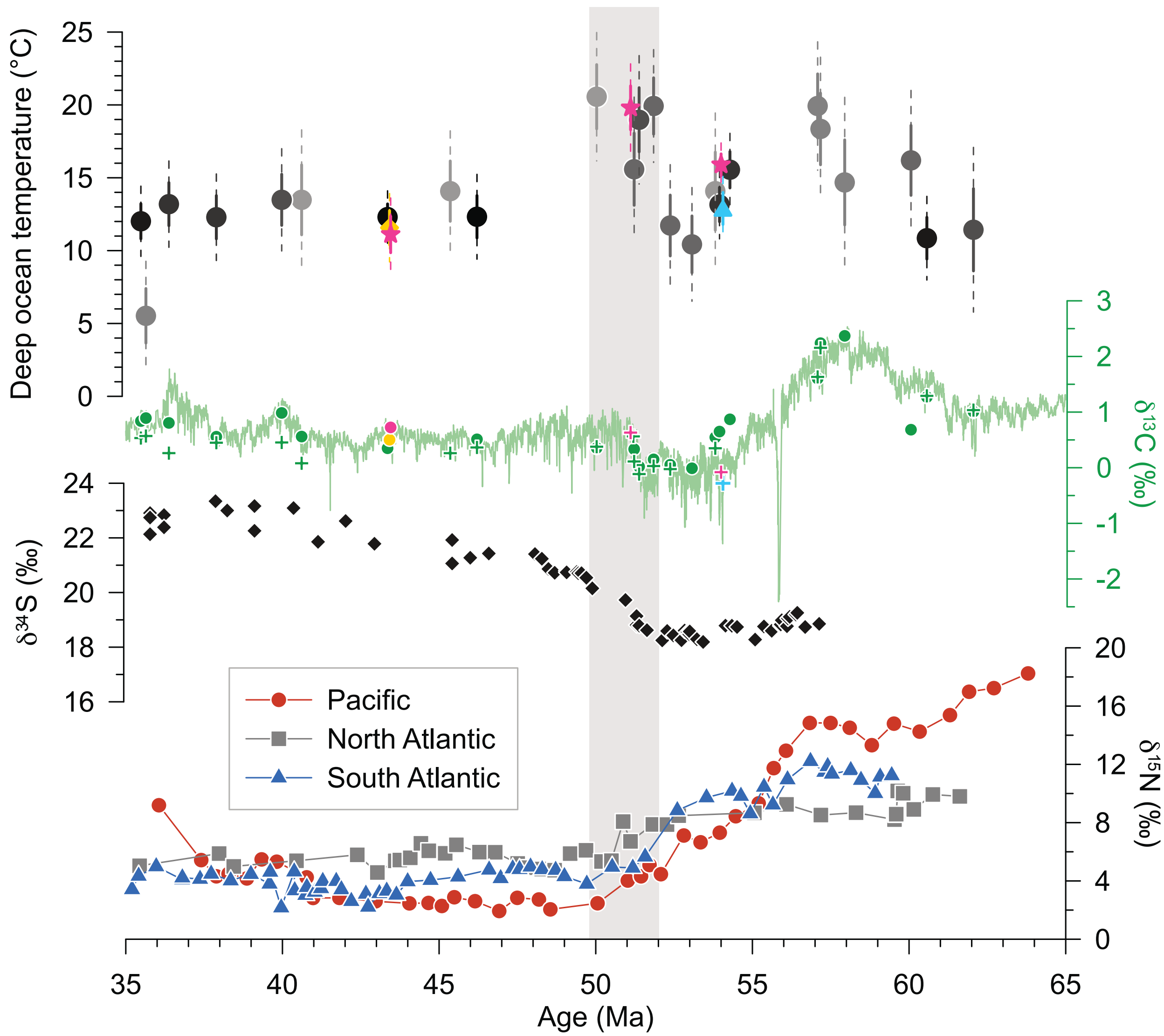

Figure S7. Comparison of the deep ocean temperatures to proxy records of biogeochemical processes for the Palocene-Eocene. $\delta^{13}C$ data are as in Fig. 1C, $\delta^{34}S$ data are from multiple sites (*34*), and $\delta^{15}N$ data are from three different sites (*35*) as indicated in the legend.

Table S1. IODP Sites from Newfoundland margin studied, with their respective water depths below sea level at present (*44*) and at 50 Ma (*45*).

Site	Present location	Water depth (m) present	Water depth (m) 50 Ma
U1407	41°25.5'N, 49°48.8'W	3074	2600
U1410	41°19.7'N, 49°10.2'W	3387	2950
U1409	41°17.7'N, 49°14.0°W	3500	3050
U1406	40°21.0'N, 51°39.0'W	3813	3300

Table S2. Site information for benthic boron isotope samples with approximate paleo water depths for the respective age intervals.

Site	Present location	Age range of benthic $\delta^{11}B$ data	Paleo water depth (m)
U1409	41°17.7'N, 49°14.0°W	53-59 Ma	2500
1258	9°26.0'N, 54°44.0°W	47-52 Ma	3200
1260	9°16.0'N, 54°33.0°W	45-46 Ma	2500
926	3°43.1'N, 42°54.5°W	5-23 Ma	3600
999	12°44.6'N, 78°44.4°W	0-3 Ma	2800

Data S1. (separate file)

Clumped isotope data averaged per sample

Data S2. (separate file)

Numbers of Δ_{47} aliquots analyzed per species/genus for each sample

Data S3. (separate file)

Deep ocean pH data from boron isotopes in benthic foraminifera

References and Notes

1. J. Zachos, M. Pagani, L. Sloan, E. Thomas, K. Billups, Trends, rhythms, and aberrations in global climate 65 Ma to present. *Science* **292**, 686–693 (2001). doi:10.1126/science.1059412 Medline

2. T. Westerhold, N. Marwan, A. J. Drury, D. Liebrand, C. Agnini, E. Anagnostou, J. S. K. Barnet, S. M. Bohaty, D. De Vleeschouwer, F. Florindo, T. Frederichs, D. A. Hodell, A. E. Holbourn, D. Kroon, V. Lauretano, K. Littler, L. J. Lourens, M. Lyle, H. Pälike, U. Röhl, J. Tian, R. H. Wilkens, P. A. Wilson, J. C. Zachos, An astronomically dated record of Earth's climate and its predictability over the last 66 million years. *Science* **369**, 1383–1387 (2020). doi:10.1126/science.aba6853 Medline

3. D. J. Lunt, F. Bragg, W.-L. Chan, D. K. Hutchinson, J.-B. Ladant, P. Morozova, I. Niezgodzki, S. Steinig, Z. Zhang, J. Zhu, A. Abe-Ouchi, E. Anagnostou, A. M. de Boer, H. K. Coxall, Y. Donnadieu, G. Foster, G. N. Inglis, G. Knorr, P. M. Langebroek, C. H. Lear, G. Lohmann, C. J. Poulsen, P. Sepulchre, J. E. Tierney, P. J. Valdes, E. M. Volodin, T. Dunkley Jones, C. J. Hollis, M. Huber, B. L. Otto-Bliesner, DeepMIP: Model intercomparison of early Eocene climatic optimum (EECO) large-scale climate features and comparison with proxy data. *Clim. Past* **17**, 203–227 (2021). doi:10.5194/cp-17-203-2021

4. K. D. Burke, J. W. Williams, M. A. Chandler, A. M. Haywood, D. J. Lunt, B. L. Otto-Bliesner, Pliocene and Eocene provide best analogs for near-future climates. *Proc. Natl. Acad. Sci. U.S.A.* **115**, 13288–13293 (2018). doi:10.1073/pnas.1809600115 Medline

5. G. N. Inglis, F. Bragg, N. J. Burls, M. J. Cramwinckel, D. Evans, G. L. Foster, M. Huber, D. J. Lunt, N. Siler, S. Steinig, J. E. Tierney, R. Wilkinson, E. Anagnostou, A. M. de Boer, T. Dunkley Jones, K. M. Edgar, C. J. Hollis, D. K. Hutchinson, R. D. Pancost, Global mean surface temperature and climate sensitivity of the early Eocene Climatic Optimum (EECO), Paleocene-Eocene Thermal Maximum (PETM), and latest Paleocene. *Clim. Past* **16**, 1953–1968 (2020). doi:10.5194/cp-16-1953-2020

6. B. S. Cramer, K. G. Miller, P. J. Barrett, J. D. Wright, Late Cretaceous-Neogene trends in deep ocean temperature and continental ice volume: Reconciling records of benthic foraminiferal geochemistry (delta O-18 and Mg/Ca) with sea level history. *J. Geophys. Res.* **116** (C12), C12023 (2011). doi:10.1029/2011JC007255

7. T. M. Marchitto, W. B. Curry, J. Lynch-Stieglitz, S. P. Bryan, K. M. Cobb, D. C. Lund, Improved oxygen isotope temperature calibrations for cosmopolitan benthic foraminifera. *Geochim. Cosmochim. Acta* **130**, 1–11 (2014). doi:10.1016/j.gca.2013.12.034

8. C. J. Hollis, T. Dunkley Jones, E. Anagnostou, P. K. Bijl, M. J. Cramwinckel, Y. Cui, G. R. Dickens, K. M. Edgar, Y. Eley, D. Evans, G. L. Foster, J. Frieling, G. N. Inglis, E. M. Kennedy, R. Kozdon, V. Lauretano, C. H. Lear, K. Littler, L. Lourens, A. N. Meckler, B. D. A. Naafs, H. Pälike, R. D. Pancost, P. N. Pearson, U. Röhl, D. L. Royer, U. Salzmann, B. A. Schubert, H. Seebeck, A. Sluijs, R. P. Speijer, P. Stassen, J. Tierney, A. Tripati, B. Wade, T. Westerhold, C. Witkowski, J. C. Zachos, Y. G. Zhang, M. Huber, D. J. Lunt, The DeepMIP contribution to PMIP4: Methodologies for selection, compilation and analysis of latest Paleocene and early Eocene climate proxy data, incorporating version

0.1 of the DeepMIP database. *Geosci. Model Dev.* **12**, 3149–3206 (2019). doi:10.5194/gmd-12-3149-2019

9. M. E. Katz, D. R. Katz, J. D. Wright, K. G. Miller, D. K. Pak, N. J. Shackleton, E. Thomas, Early Cenozoic benthic foraminiferal isotopes: Species reliability and interspecies correction factors. *Paleoceanography* **18**, 1024 (2003). doi:10.1029/2002PA000798

10. A. Tripati, J. Backman, H. Elderfield, P. Ferretti, Eocene bipolar glaciation associated with global carbon cycle changes. *Nature* **436**, 341–346 (2005). doi:10.1038/nature03874 Medline

11. C. H. Lear, H. Elderfield, P. A. Wilson, Cenozoic deep-Sea temperatures and global ice volumes from Mg/Ca in benthic foraminiferal calcite. *Science* **287**, 269–272 (2000). doi:10.1126/science.287.5451.269 Medline

12. C. H. Lear, E. M. Mawbey, Y. Rosenthal, Cenozoic benthic foraminiferal Mg/Ca and Li/Ca records: Toward unlocking temperatures and saturation states. *Paleoceanography* **25**, PA4215 (2010). doi:10.1029/2009PA001880

13. J. M. Eiler, "Clumped-isotope" geochemistry - The study of naturally-occurring, multiply-substituted isotopologues. *Earth Planet. Sci. Lett.* **262**, 309–327 (2007). doi:10.1016/j.epsl.2007.08.020

14. S. Bernard, D. Daval, P. Ackerer, S. Pont, A. Meibom, Burial-induced oxygen-isotope re-equilibration of fossil foraminifera explains ocean paleotemperature paradoxes. *Nat. Commun.* **8**, 1134 (2017). doi:10.1038/s41467-017-01225-9 Medline

15. D. Evans, M. P. S. Badger, G. L. Foster, M. J. Henehan, C. H. Lear, J. C. Zachos, No substantial long-term bias in the Cenozoic benthic foraminifera oxygen-isotope record. *Nat. Commun.* **9**, 2875 (2018). doi:10.1038/s41467-018-05303-4 Medline

16. S. E. Modestou, T. J. Leutert, A. Fernandez, C. H. Lear, A. N. Meckler, Warm Middle Miocene Indian Ocean bottom water temperatures: Comparison of clumped isotope and Mg/Ca-based estimates. *Paleoceanogr. Paleoclimatol.* **35**, e2020PA003927 (2020). doi:10.1029/2020PA003927

17. T. J. Leutert, S. Modestou, S. M. Bernasconi, A. N. Meckler, Southern Ocean bottom-water cooling and ice sheet expansion during the middle Miocene climate transition. *Clim. Past* **17**, 2255–2271 (2021). doi:10.5194/cp-17-2255-2021

18. T. Agterhuis, M. Ziegler, N. J. de Winter, L. J. Lourens, Warm deep-sea temperatures across Eocene Thermal Maximum 2 from clumped isotope thermometry. *Commun. Earth Environ* **3**, 39 (2022). doi:10.1038/s43247-022-00350-8

19. T. J. Leutert, P. F. Sexton, A. Tripati, A. Piasecki, S. L. Ho, A. N. Meckler, Sensitivity of clumped isotope temperatures in fossil benthic and planktic foraminifera to diagenetic alteration. *Geochim. Cosmochim. Acta* **257**, 354–372 (2019). doi:10.1016/j.gca.2019.05.005

20. N. Thiagarajan, A. V. Subhas, J. R. Southon, J. M. Eiler, J. F. Adkins, Abrupt pre-Bølling-Allerød warming and circulation changes in the deep ocean. *Nature* **511**, 75–78 (2014). doi:10.1038/nature13472 Medline

21. R. D. Müller, M. Sdrolias, C. Gaina, B. Steinberger, C. Heine, Long-term sea-level fluctuations driven by ocean basin dynamics. *Science* **319**, 1357–1362 (2008). doi:10.1126/science.1151540 Medline

22. J. E. Wendler, I. Wendler, C. Vogt, J. Kuss, Link between cyclic eustatic sea-level change and continental weathering: Evidence for aquifer-eustasy in the Cretaceous. *Palaeogeogr. Palaeoclimatol. Palaeoecol.* **441**, 430–437 (2016). doi:10.1016/j.palaeo.2015.08.014

23. A. Davies, B. Gréselle, S. J. Hunter, G. Baines, C. Robson, A. M. Haywood, D. C. Ray, M. D. Simmons, F. S. P. van Buchem, Assessing the impact of aquifer-eustasy on short-term Cretaceous sea-level. *Cretac. Res.* **112**, 104445 (2020). doi:10.1016/j.cretres.2020.104445

24. J. W. B. Rae, Y. G. Zhang, X. Liu, G. L. Foster, H. M. Stoll, R. D. M. Whiteford, Atmospheric CO_2 over the past 66 million years from marine archives. *Annu. Rev. Earth Planet. Sci.* **49**, 609–641 (2021). doi:10.1146/annurev-earth-082420-063026

25. E. Anagnostou, E. H. John, T. L. Babila, P. F. Sexton, A. Ridgwell, D. J. Lunt, P. N. Pearson, T. B. Chalk, R. D. Pancost, G. L. Foster, Proxy evidence for state-dependence of climate sensitivity in the Eocene greenhouse. *Nat. Commun.* **11**, 4436 (2020). doi:10.1038/s41467-020-17887-x Medline

26. R. E. Zeebe, Seawater pH and isotopic paleotemperatures of Cretaceous oceans. *Palaeogeogr. Palaeoclimatol. Palaeoecol.* **170**, 49–57 (2001). doi:10.1016/S0031-0182(01)00226-7

27. H. J. Spero, J. Bijma, D. W. Lea, B. E. Bemis, Effect of seawater carbonate concentration on foraminiferal carbon and oxygen isotopes. *Nature* **390**, 497–500 (1997). doi:10.1038/37333

28. A. K. Tripati, P. S. Hill, R. A. Eagle, J. L. Mosenfelder, J. Tang, E. A. Schauble, J. M. Eiler, R. E. Zeebe, J. Uchikawa, T. B. Coplen, J. B. Ries, D. Henry, Beyond temperature: Clumped isotope signatures in dissolved inorganic carbon species and the influence of solution chemistry on carbonate mineral composition. *Geochim. Cosmochim. Acta* **166**, 344–371 (2015). doi:10.1016/j.gca.2015.06.021

29. W. F. Guo, Kinetic clumped isotope fractionation in the DIC-H_2O-CO_2 system: Patterns, controls, and implications. *Geochim. Cosmochim. Acta* **268**, 230–257 (2020). doi:10.1016/j.gca.2019.07.055

30. J. W. Tang, M. Dietzel, A. Fernandez, A. K. Tripati, B. E. Rosenheim, Evaluation of kinetic effects on clumped isotope fractionation (Delta(47)) during inorganic calcite precipitation. *Geochim. Cosmochim. Acta* **134**, 120–136 (2014). doi:10.1016/j.gca.2014.03.005

31. K. K. Śliwińska, E. Thomsen, S. Schouten, P. L. Schoon, C. Heilmann-Clausen, Climate- and gateway-driven cooling of Late Eocene to earliest Oligocene sea surface temperatures in the North Sea Basin. *Sci. Rep.* **9**, 4458 (2019). doi:10.1038/s41598-019-41013-7 Medline

32. M. L. Vickers, S. K. Lengger, S. M. Bernasconi, N. Thibault, B. P. Schultz, A. Fernandez, C. V. Ullmann, P. McCormack, C. J. Bjerrum, J. A. Rasmussen, I. W. Hougård, C. Korte,

Cold spells in the Nordic Seas during the early Eocene Greenhouse. *Nat. Commun.* **11**, 4713 (2020). doi:10.1038/s41467-020-18558-7 Medline

33. C. Gaina, J. Jakob, Global Eocene tectonic unrest: Possible causes and effects around the North American plate. *Tectonophysics* **760**, 136–151 (2019). doi:10.1016/j.tecto.2018.08.010

34. V. C. F. Rennie, G. Paris, A. L. Sessions, S. Abramovich, A. V. Turchyn, J. F. Adkins, Cenozoic record of delta S-34 in foraminiferal calcite implies an early Eocene shift to deep-ocean sulfide burial. *Nat. Geosci.* **11**, 761–765 (2018). doi:10.1038/s41561-018-0200-y

35. E. R. Kast, D. A. Stolper, A. Auderset, J. A. Higgins, H. Ren, X. T. Wang, A. Martínez-García, G. H. Haug, D. M. Sigman, Nitrogen isotope evidence for expanded ocean suboxia in the early Cenozoic. *Science* **364**, 386–389 (2019). doi:10.1126/science.aau5784 Medline

36. J. Lynch-Stieglitz, W. B. Curry, N. Slowey, A geostrophic transport estimate for the Florida Current from the oxygen isotope composition of benthic foraminifera. *Paleoceanography* **14**, 360–373 (1999). doi:10.1029/1999PA900001

37. J. Zhu, C. J. Poulsen, B. L. Otto-Bliesner, Z. Liu, E. C. Brady, D. C. Noone, Simulation of early Eocene water isotopes using an Earth system model and its implication for past climate reconstruction. *Earth Planet. Sci. Lett.* **537**, 116164 (2020). doi:10.1016/j.epsl.2020.116164

38. A. Tripati, H. Elderfield, Deep-sea temperature and circulation changes at the Paleocene-Eocene Thermal Maximum. *Science* **308**, 1894–1898 (2005). doi:10.1126/science.1109202 Medline

39. P. M. J. Douglas, H. P. Affek, L. C. Ivany, A. J. P. Houben, W. P. Sijp, A. Sluijs, S. Schouten, M. Pagani, Pronounced zonal heterogeneity in Eocene southern high-latitude sea surface temperatures. *Proc. Natl. Acad. Sci. U.S.A.* **111**, 6582–6587 (2014). doi:10.1073/pnas.1321441111 Medline

40. R. Greenop, M. P. Hain, S. M. Sosdian, K. I. C. Oliver, P. Goodwin, T. B. Chalk, C. H. Lear, P. A. Wilson, G. L. Foster, A record of Neogene seawater δ^{11}B reconstructed from paired δ^{11}B analyses on benthic and planktic foraminifera. *Clim. Past* **13**, 149–170 (2017). doi:10.5194/cp-13-149-2017

41. A. N. Meckler, P. F. Sexton, A. M. Piasecki, T. J. Leutert, J. Marquardt, M. Ziegler, T. Agterhuis, L. J. Lourens, J. W. B. Rae, J. Barnet, A. Tripati, S. M. Bernasconi, Cenozoic clumped isotope temperature record from the deep North Atlantic for: Cenozoic evolution of deep ocean temperature from clumped isotope thermometry, Version 1.0, EarthChem (2022); https://doi.org/10.26022/IEDA/112213.

42. A. N. Meckler, P. F. Sexton, A. M. Piasecki, T. J. Leutert, J. Marquardt, M. Ziegler, T. Agterhuis, L. J. Lourens, J. W. B. Rae, J. Barnet, A. Tripati, S. M. Bernasconi, Clumped isotope deep-sea temperature data in the South Atlantic for the Early Eocene Climatic Optimum from Meckler et al. (2022) for: Cenozoic evolution of deep ocean temperature from clumped isotope thermometry, Version 1.0, EarthChem (2022); https://doi.org/10.26022/IEDA/112215.

43. A. N. Meckler, P. F. Sexton, A. M. Piasecki, T. J. Leutert, J. Marquardt, M. Ziegler, T. Agterhuis, L. J. Lourens, J. W. B. Rae, J. Barnet, A. Tripati, S. M. Bernasconi, Cenozoic clumped isotope temperature record from the deep North Atlantic for: Cenozoic evolution of deep ocean temperature from clumped isotope thermometry, Pangaea (2022); https://doi.org/10.1594/PANGAEA.945578.

44. Integrated Ocean Drilling Program, Paleogene Newfoundland sediment drifts. Expedition 342 (IODP, 2012); https://iodp.tamu.edu/scienceops/expeditions/newfoundland_sediment_drifts.html.

45. B. E. Tucholke, P. R. Vogt, "Western North Atlantic: Sedimentary evolution and aspects of tectonic history," in *DSDP Initial Reports,* B. Tucholke, P. R. Vogt, Eds. (US Government Printing Office, 1979), vol. 43, pp. 791–825; http://deepseadrilling.org/43/volume/dsdp43_40.pdf.

46. N. Meinicke, S. L. Ho, B. Hannisdal, D. Nürnberg, A. Tripati, R. Schiebel, A. N. Meckler, A robust calibration of the clumped isotopes to temperature relationship for foraminifers. *Geochim. Cosmochim. Acta* **270**, 160–183 (2020). doi:10.1016/j.gca.2019.11.022

47. A. K. Tripati, R. A. Eagle, N. Thiagarajan, A. C. Gagnon, H. Bauch, P. R. Halloran, J. M. Eiler, C-13-O-18 isotope signatures and 'clumped isotope' thermometry in foraminifera and coccoliths. *Geochim. Cosmochim. Acta* **74**, 5697–5717 (2010). doi:10.1016/j.gca.2010.07.006

48. A. L. Grauel, T. W. Schmid, B. Hu, C. Bergami, L. Capotondi, L. Zhou, S. M. Bernasconi, Calibration and application of the 'clumped isotope' thermometer to foraminifera for high-resolution climate reconstructions. *Geochim. Cosmochim. Acta* **108**, 125–140 (2013). doi:10.1016/j.gca.2012.12.049

49. A. Piasecki, S. M. Bernasconi, A.-L. Grauel, B. Hannisdal, S. L. Ho, T. J. Leutert, T. M. Marchitto, N. Meinicke, A. Tisserand, N. Meckler, Application of clumped isotope thermometry to benthic foraminifera. *Geochem. Geophys. Geosyst.* **20**, 2082–2090 (2019). doi:10.1029/2018GC007961

50. M. Peral, M. Daëron, D. Blamart, F. Bassinot, F. Dewilde, N. Smialkowski, G. Isguder, J. Bonnin, F. Jorissen, C. Kissel, E. Michel, N. Vázquez Riveiros, C. Waelbroeck, Updated calibration of the clumped isotope thermometer in planktonic and benthic foraminifera. *Geochim. Cosmochim. Acta* **239**, 1–16 (2018). doi:10.1016/j.gca.2018.07.016

51. D. A. Stolper, J. M. Eiler, J. A. Higgins, Modeling the effects of diagenesis on carbonate clumped-isotope values in deep- and shallow-water settings. *Geochim. Cosmochim. Acta* **227**, 264–291 (2018). doi:10.1016/j.gca.2018.01.037

52. S. M. Bernasconi, I. A. Müller, K. D. Bergmann, S. F. M. Breitenbach, A. Fernandez, D. A. Hodell, M. Jaggi, A. N. Meckler, I. Millan, M. Ziegler, Reducing uncertainties in carbonate clumped isotope analysis through consistent carbonate-based standardization. *Geochem. Geophys. Geosyst.* **19**, 2895–2914 (2018). doi:10.1029/2017GC007385 Medline

53. A. N. Meckler, M. Ziegler, M. I. Millán, S. F. M. Breitenbach, S. M. Bernasconi, Long-term performance of the Kiel carbonate device with a new correction scheme for clumped

isotope measurements. *Rapid Commun. Mass Spectrom.* **28**, 1705–1715 (2014). doi:10.1002/rcm.6949 Medline

54. B. Hu, J. Radke, H.-J. Schlüter, F. T. Heine, L. Zhou, S. M. Bernasconi, A modified procedure for gas-source isotope ratio mass spectrometry: The long-integration dual-inlet (LIDI) methodology and implications for clumped isotope measurements. *Rapid Commun. Mass Spectrom.* **28**, 1413–1425 (2014). doi:10.1002/rcm.6909 Medline
55. S. M. Bernasconi, M. Daëron, K. D. Bergmann, M. Bonifacie, A. N. Meckler, H. P. Affek, N. Anderson, D. Bajnai, E. Barkan, E. Beverly, D. Blamart, L. Burgener, D. Calmels, C. Chaduteau, M. Clog, B. Davidheiser-Kroll, A. Davies, F. Dux, J. Eiler, B. Elliott, A. C. Fetrow, J. Fiebig, S. Goldberg, M. Hermoso, K. W. Huntington, E. Hyland, M. Ingalls, M. Jaggi, C. M. John, A. B. Jost, S. Katz, J. Kelson, T. Kluge, I. J. Kocken, A. Laskar, T. J. Leutert, D. Liang, J. Lucarelli, T. J. Mackey, X. Mangenot, N. Meinicke, S. E. Modestou, I. A. Müller, S. Murray, A. Neary, N. Packard, B. H. Passey, E. Pelletier, S. Petersen, A. Piasecki, A. Schauer, K. E. Snell, P. K. Swart, A. Tripati, D. Upadhyay, T. Vennemann, I. Winkelstern, D. Yarian, N. Yoshida, N. Zhang, M. Ziegler, InterCarb: A community effort to improve interlaboratory standardization of the carbonate clumped isotope thermometer using carbonate standards. *Geochem. Geophys. Geosyst.* **22**, GC009588 (2021). doi:10.1029/2020GC009588 Medline
56. C. M. John, D. Bowen, Community software for challenging isotope analysis: First applications of 'Easotope' to clumped isotopes. *Rapid Commun. Mass Spectrom.* **30**, 2285–2300 (2016). doi:10.1002/rcm.7720 Medline
57. N. Meinicke, M. A. Reimi, A. C. Ravelo, A. N. Meckler, Coupled Mg/Ca and clumped isotope measurements confirm lack of substantial mixed layer cooling in the Western Pacific warm pool over the last 5 million years. *Paleoceanogr. Paleoclimatol.* **36**, e2020PA004115 (2021). doi:10.1029/2020PA004115
58. S. Kele, S. F. M. Breitenbach, E. Capezzuoli, A. N. Meckler, M. Ziegler, I. M. Millan, T. Kluge, J. Deák, K. Hanselmann, C. M. John, H. Yan, Z. Liu, S. M. Bernasconi, Temperature dependence of oxygen- and clumped isotope fractionation in carbonates: A study of travertines and tufas in the 6–95°C temperature range. *Geochim. Cosmochim. Acta* **168**, 172–192 (2015). doi:10.1016/j.gca.2015.06.032
59. N. T. Anderson, J. R. Kelson, S. Kele, M. Daëron, M. Bonifacie, J. Horita, T. J. Mackey, C. M. John, T. Kluge, P. Petschnig, A. B. Jost, K. W. Huntington, S. M. Bernasconi, K. D. Bergmann, A unified clumped isotope thermometer calibration (0.5-1,100 degrees C) using carbonate-based standardization. *Geophys. Res. Lett.* **48**, e2020GL092069 (2021). doi:10.1029/2020GL092069
60. W. F. Guo, J. L. Mosenfelder, W. A. Goddard III, J. M. Eiler, Isotopic fractionations associated with phosphoric acid digestion of carbonate minerals: Insights from firstprinciples theoretical modeling and clumped isotope measurements. *Geochim. Cosmochim. Acta* **73**, 7203–7225 (2009). doi:10.1016/j.gca.2009.05.071
61. J. W. B. Rae, W. Broecker, What fraction of the Pacific and Indian oceans' deep water is formed in the Southern Ocean? *Biogeosciences* **15**, 3779–3794 (2018). doi:10.5194/bg-15-3779-2018

62. J. W. B. Rae, G. L. Foster, D. N. Schmidt, T. Elliott, Boron isotopes and B/Ca in benthic foraminifera: Proxies for the deep ocean carbonate system. *Earth Planet. Sci. Lett.* **302**, 403–413 (2011). doi:10.1016/j.epsl.2010.12.034

63. J. W. B. Rae, A. Burke, L. F. Robinson, J. F. Adkins, T. Chen, C. Cole, R. Greenop, T. Li, E. F. M. Littley, D. C. Nita, J. A. Stewart, B. J. Taylor, CO_2 storage and release in the deep Southern Ocean on millennial to centennial timescales. *Nature* **562**, 569–573 (2018). doi:10.1038/s41586-018-0614-0 Medline

64. G. L. Foster, B. Hönisch, G. Paris, G. S. Dwyer, J. W. B. Rae, T. Elliott, J. Gaillardet, N. G. Hemming, P. Louvat, A. Vengosh, Interlaboratory comparison of boron isotope analyses of boric acid, seawater and marine CaCO3 by MC-ICPMS and NTIMS. *Chem. Geol.* **358**, 1–14 (2013). doi:10.1016/j.chemgeo.2013.08.027

65. M. Gutjahr, L. Bordier, E. Douville, J. Farmer, G. L. Foster, E. C. Hathorne, B. Hönisch, D. Lemarchand, P. Louvat, M. McCulloch, J. Noireaux, N. Pallavicini, J. W. B. Rae, I. Rodushkin, P. Roux, J. A. Stewart, F. Thil, C.-F. You, Sub-Permil Interlaboratory Consistency for Solution-Based Boron Isotope Analyses on Marine Carbonates. *Geostand. Geoanal. Res.* **45**, 59–75 (2021). doi:10.1111/ggr.12364

66. J. A. Stewart, L. F. Robinson, R. D. Day, I. Strawson, A. Burke, J. W. B. Rae, P. T. Spooner, A. Samperiz, P. J. Etnoyer, B. Williams, A. Paytan, M. J. Leng, V. Häussermann, L. N. Wickes, R. Bratt, H. Pryer, Refining trace metal temperature proxies in cold-water scleractinian and stylasterid corals. *Earth Planet. Sci. Lett.* **545**, 116412 (2020). doi:10.1016/j.epsl.2020.116412

67. J. W. B. Rae, "Boron isotopes in Foraminifera: Systematics, biomineralisation, and CO_2 reconstruction," in *Boron Isotopes: The Fifth Element (Advances in Isotope Geochemistry*, H. Marschall, G. Foster, Eds. (Springer, 2018), pp. 107–143.

68. S. T. Brennan, T. K. Lowenstein, D. I. Cendon, The major-ion composition of Cenozoic seawater: The past 36 million years from fluid inclusions in marine halite. *Am. J. Sci.* **313**, 713–775 (2013). doi:10.2475/08.2013.01

69. M. P. Hain, D. M. Sigman, J. A. Higgins, G. H. Haug, The effects of secular calcium and magnesium concentration changes on the thermodynamics of seawater acid/base chemistry: Implications for Eocene and Cretaceous ocean carbon chemistry and buffering. *Global Biogeochem. Cycles* **29**, 517–533 (2015). doi:10.1002/2014GB004986

70. J. Frieling, A. I. Iakovleva, G.-J. Reichart, G. N. Aleksandrova, Z. N. Gnibidenko, S. Schouten, A. Sluijs, Paleocene-Eocene warming and biotic response in the epicontinental West Siberian Sea. *Geology* **42**, 767–770 (2014). doi:10.1130/G35724.1

71. J. Frieling, G.-J. Reichart, J. J. Middelburg, U. Röhl, T. Westerhold, S. M. Bohaty, A. Sluijs, Tropical Atlantic climate and ecosystem regime shifts during the Paleocene-Eocene Thermal Maximum. *Clim. Past* **14**, 39–55 (2018). doi:10.5194/cp-14-39-2018

72. M. J. Cramwinckel, M. Huber, I. J. Kocken, C. Agnini, P. K. Bijl, S. M. Bohaty, J. Frieling, A. Goldner, F. J. Hilgen, E. L. Kip, F. Peterse, R. van der Ploeg, U. Röhl, S. Schouten, A. Sluijs, Synchronous tropical and polar temperature evolution in the Eocene. *Nature* **559**, 382–386 (2018). doi:10.1038/s41586-018-0272-2 Medline

73. C. J. Hollis, K. W. R. Taylor, L. Handley, R. D. Pancost, M. Huber, J. B. Creech, B. R. Hines, E. M. Crouch, H. E. G. Morgans, J. S. Crampton, S. Gibbs, P. N. Pearson, J. C. Zachos, Early Paleogene temperature history of the Southwest Pacific Ocean: Reconciling proxies and models. *Earth Planet. Sci. Lett.* **349**, 53–66 (2012). doi:10.1016/j.epsl.2012.06.024

74. P. K. Bijl, S. Schouten, A. Sluijs, G.-J. Reichart, J. C. Zachos, H. Brinkhuis, Early Palaeogene temperature evolution of the southwest Pacific Ocean. *Nature* **461**, 776–779 (2009). doi:10.1038/nature08399 Medline

75. P. K. Bijl, J. A. P. Bendle, S. M. Bohaty, J. Pross, S. Schouten, L. Tauxe, C. E. Stickley, R. M. McKay, U. Röhl, M. Olney, A. Sluijs, C. Escutia, H. Brinkhuis, Expedition 318 Scientists, A. Klaus, A. Fehr, T. Williams, S. A. Carr, R. B. Dunbar, J. J. Gonzàlez, T. G. Hayden, M. Iwai, F. J. Jimenez-Espejo, K. Katsuki, G. S. Kong, M. Nakai, S. Passchier, S. F. Pekar, C. Riesselman, T. Sakai, P. K. Shrivastava, S. Sugisaki, S. Tuo, T. van de Flierdt, K. Welsh, M. Yamane, Eocene cooling linked to early flow across the Tasmanian Gateway. *Proc. Natl. Acad. Sci. U.S.A.* **110**, 9645–9650 (2013). doi:10.1073/pnas.1220872110 Medline

76. A. Sluijs, P. K. Bijl, S. Schouten, U. Röhl, G.-J. Reichart, H. Brinkhuis, Southern ocean warming, sea level and hydrological change during the Paleocene-Eocene thermal maximum. *Clim. Past* **7**, 47–61 (2011). doi:10.5194/cp-7-47-2011

77. G. N. Inglis, A. Farnsworth, D. Lunt, G. L. Foster, C. J. Hollis, M. Pagani, P. E. Jardine, P. N. Pearson, P. Markwick, A. M. J. Galsworthy, L. Raynham, K. W. R. Taylor, R. D. Pancost, Descent toward the Icehouse: Eocene sea surface cooling inferred from GDGT distributions. *Paleoceanography* **30**, 1000–1020 (2015). doi:10.1002/2014PA002723

78. A. K. Tripati, M. L. Delaney, J. C. Zachos, L. D. Anderson, D. C. Kelly, H. Elderfield, Tropical sea-surface temperature reconstruction for the early Paleogene using Mg/Ca ratios of planktonic foraminifera. *Paleoceanography* **18**, 1101 (2003). doi:10.1029/2003PA000937

79. J. Hansen, M. Sato, G. Russell, P. Kharecha, Climate sensitivity, sea level and atmospheric carbon dioxide. *Philos. Trans. A Math. Phys. Eng. Sci.* **371**, 20120294 (2013). doi:10.1098/rsta.2012.0294 Medline